QSS: Quantum Spectrum Sensing for CRN-NOMA using Data Re-uploading VQC

Moniruzzaman[1], Avi Deb Raha[2], Eui-Nam Huh[2], and Choong Seon Hong[2]*
[1]Department of Artificial Intelligence, Kyung Hee University, Yongin-si, Republic of Korea
[2]Department of Computer Science and Engineering, Kyung Hee University, Yongin-si, Republic of Korea
Email: {monir, avi, johnhuh, cshong}@khu.ac.kr

***Abstract*—In contemporary times, it is nearly impossible to function without mobile devices, along with various technologies of daily use such as smartwatches, home assistants, smart car keys, and many more. All these types of devices use wideband wireless services for communication. With the limited resource of wideband spectrum, it is not possible to provide service to the growing demands. The challenge lies in efficiently conducting the sensing and sharing of the spectrum. Consequently, the cognitive radio network (CRN) is experiencing increasing demand due to its innovative mechanisms for spectrum sensing. Moreover, non-orthogonal multiple access (NOMA) in CRN improves the spectrum utilization in wireless communications. However, spectrum sensing becomes increasingly critical and intricate in the scenario involving CRN-NOMA. Numerous initiatives have been taken to enhance the detection of the CRN spectrum and improve overall performance. Nevertheless, the existing literature highlights a shortcoming in performance at low Signal-to-Noise Ratio (SNR) levels, a concern of particular importance due to the considerable noise inherent within the communication medium. In this study, we utilized variational quantum circuits (VQCs) tailored for the noisy intermediate-scale quantum (NISQ) era. The proposed model leverages the capabilities of a convolutional neural network (CNN) to capture standout features, VQC are employed, with additional expressivity achieved via data re-uploading within the variable layer, resulting in improved performance metrics. Ultimately, to demonstrate the efficacy of our model, we conducted experiments and performed comparisons with several state-of-the-art baselines. The findings indicate that the proposed model consistently surpasses the performance of baseline models, especially within low SNR conditions, achieving detection performance close to the optimal level, and showcasing substantial robustness in environments with significant noise interference.**

***Index Terms*—Quantum spectrum sensing, Data reuploading, CNN, Low-SNR sensing, CRN, NOMA**

I. Introduction

Wireless systems rely on electromagnetic spectrum to carry the signals, and without spectrum, no wireless transmission is possible. The spectrum is finite, and only a certain frequency range is suitable for communication. So, syncing different spectrum for different countries for different organizations is very difficult and complicated. Cognitive radio networks (CRNs) and non-orthogonal multiple access (NOMA) are both pivotal innovations in improving spectrum utilization in wireless communications. CRNs enable dynamic spectrum access by allowing secondary (unlicensed) users to opportunistically use underutilized frequency bands when primary (licensed) users are idle [1]. NOMA, on the other hand, improves spectral efficiency by allowing multiple users to share the same time-frequency resources through multiplexing in the power domain or the code domain [2]. In a CRN-NOMA system, secondary users can transmit simultaneously at different power levels, potentially increasing network capacity and connectivity without exclusive spectrum allocation. However, this integration also presents significant challenges. Already in CRN various forms of interference are inherent, including cross-tier interference at both the primary users (PU) and secondary users (SU), and intra-secondary interference. The overlapping signal structure of NOMA creates interference within the cell between users of different power levels, complicating the classic cognitive radio (CR) task of detecting whether a channel is free. Consequently, spectrum sensing, which involves the detection of unused spectrum by CR nodes, becomes increasingly critical and intricate in scenarios involving CRN-NOMA. Fortunately, researchers have devised methods to address these challenges effectively. Traditional spectrum sensing techniques, energy detection (ED), matched filtering (MF), and cyclostationary detection (CSD), baseline parameters to remain consistent, but require interface-aware thresholding under NOMA [2]. Wu *et al.* [3] develop an adaptive thresholding mechanism that correlates the probability of detection (P_d) and the probability of false alarm (P_f) with user activity and power allocation, thus enhancing throughput in IoT uplinks. Wu's adaptive sensing method led to a substantial improvement in system throughput.

Furthermore, a significant limitation of conventional ED and MF is their suboptimal performance in environments characterized by low signal-to-noise ratios (SNR) or non-stationary signal conditions, which are prevalent in NOMA scenarios. Deep learning models excel at learning complex signal patterns and distinguishing overlapping signals. Recurrent neural networks (RNNs) and convolutional neural networks (CNNs) have been applied to detect spectral occupancy in NOMA waveforms [2], [4]–[7]. Kumar et al. [2] proposed the

This work was supported by the National Research Foundation of Korea(NRF) grant funded by the Korea government(MSIT) (No. RS-2024-00352423) and part by Institute of Information & communications Technology Planning & Evaluation (IITP) grant funded by the Korea government(MSIT) (No.2019-0-01287, Evolvable Deep Learning Model Generation Platform for Edge Computing) and part by IITP(Institute of Information & Coummunications Technology Planning & Evaluation)-ITRC(Information Technology Research Center) grant funded by the Korea government(Ministry of Science and ICT) (IITP-2025-RS-2023-00258649) *Dr. CS Hong is the corresponding author.

RNN-BiLSTM model to sense NOMA signals under fading conditions. The model uses sequential learning to discern subtle characteristics of the signals of the primary users, even when these signals are intertwined with secondary transmissions. The RNN-BiLSTM model achieved an almost perfect detection probability at -5 dB, while a traditional energy detector needed over +2 dB SNR for comparable results. Researchers continue to advance these models by combining neural networks with conventional detectors. Neural networks dynamically adjust the thresholds in the energy detectors or the output of the matched filters, showing significant improvements in detection accuracy and reliability over traditional methods [3]. The reinforcement learning (RL) variants optimize the scheduling of sensing activities and the selection of access modes to enhance long-term throughput while adhering to interference constraints, as examined in [8].

In case of a more recent trend in networking, quantum annealing is used in active user detection (AUD) in NOMA by mapping AUD to an Ising Hamiltonian, showing efficient runtimes in code-domain scenarios and potential for CRN-NOMA decision tasks [9]. For radio resource decisions, quantum inspired evolutionary algorithms (QEA) improve NOMA user pairing versus classical heuristics, increasing the sum rate with lightweight operators [10].

Evidence in recent works [2], [3] indicates that ML-assisted detection unlocks the promised gains in the spectral efficiency of CRN-NOMA. Priorities now include standardizing datasets, benchmarks, and open-set robustness toward 6G. This study focused on enhancing spectrum sensing methods using variational quantum circuits (VQC), where a data-reuploading mechanism is applied for a more expressive model. Employing this model, the CR node effectively allocates the spectrum to SUs. A synopsis of our contributions is presented as follows:

- Initially, we introduced a simulated scenario for NOMA signals within the framework of CRN.
- Secondly, by utilizing the data re-uploading method within VQCs, we constructed a convolutional quantum neural network for spectrum sensing.
- Finally, to demonstrate the efficacy of our model in spectrum sensing, we conducted experiments and performed comparisons with several state-of-the-art baselines in the domain of spectrum sensing.

II. System Model

The main communication in CRN-NOMA architecture is built on the interaction of two tiers of users and their respective base stations. There are two types of networks. In Fig. 1(a), the primary and secondary networks are illustrated. In the primary network (PN), PUs communicate through licensed spectrum with priority access to the channel. PUs are served by the primary base station (PBS) and are protected from harmful interference. However, secondary networks (SNs) are the cognitive network. SUs are served by the secondary base station (SBS), also known as the cognitive base station (CBS). As in PBS, CBS has no specific spectrum for different

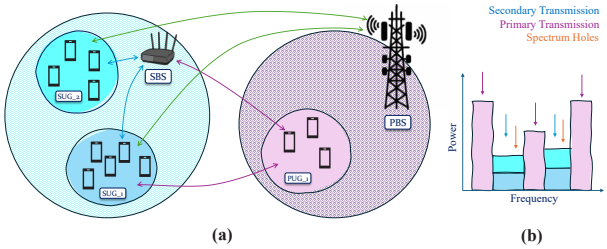

Fig. 1. The architecture of cognitive radio networks with non-orthogonal multiple access (CRN-NOMA) is illustrated, where purple denotes the primary network and aqua represents the secondary network.

secondary user groups (SUGs), it has to rely on opportunistic spectrum sharing.

The proposed method used CRN in interwave mode. Fig. 1(b) shows the operating paradigm in CRN with NOMA power domain NOMA. In this architecture, SNs serve multiple SUs with different power levels. The frame structure consists of a sensing slot and a data transmission slot. CBS performs spectrum sensing to detect PU activity before accessing the spectrum. This sensing process is formulated and executed within a statistical hypothesis testing framework:

$$\mathcal{H}_0 : y(t) = n(t), \tag{1}$$

$$\mathcal{H}_1 : y(t) = hs(s) + n(t) \tag{2}$$

where h is the channel coefficient between PU and the cognitive receiver that performs the sensing, $n(t)$ models the receiver noise and $s(t)$ denotes the PU signal. Detection is typically performed using energy detection, where the decision statistic is compared against a predefined threshold. Eq. 3 is the energy detector test statistics for N number of samples.

$$T = \frac{1}{N}\sum_{i=1}^{n} |y(i)|^2 \tag{3}$$

where the decision rule with threshold λ is

$$T \underset{\mathcal{H}_0}{\overset{\mathcal{H}_1}{\gtrless}} \lambda \tag{4}$$

Therefore, λ should be selected with an optimistic approach, as otherwise a poor spectrum sensing process can lead to erroneously concluding that the PUs are inactive. To eradicate this issue, CRN-NOMA demands a better spectrum sensing detection mechanism. Two other important phenomena in CRN-NOMA, P_d and P_f that help to make the optimal detection mechanism. P_d represents the probability of correctly identifying that the "PU is present," as illustrated in Eq. 6, while P_f refers to the detection circumstance where the "PU is present," yet the communication band remains unutilized, as outlined in Eq. 5.

$$P_f(\lambda) = Q\left(\frac{\lambda/\sigma^2 - 1}{\sqrt{2/N}}\right) \tag{5}$$

$$P_d(\lambda, \gamma) = Q\left(\frac{\lambda/\sigma^2 - (1+\gamma)}{\sqrt{2(1+2\gamma)/N}}\right) \tag{6}$$

A high P_d setting ensures minimal interference with PUs, while a low P_f setting optimizes SU utilization to achieve maximum throughput. Our experiment involves plotting a receiver operating characteristic (ROC) curve for PUs to evaluate the effectiveness of the chosen method λ in various SNRs. Hence, the ROC curves demonstrate the balance between P_d and P_f, providing an assessment of the performance of our model. The primary objective of the proposed CRN-NOMA system is to achieve precise spectrum detection, thereby improving the overall efficiency of spectrum utilization.

III. Simulation of Uplink NOMA Dataset Generation

This section describes the simulation procedure used to generate the uplink dataset for spectrum sensing in a NOMA environment. The proposed feature-based spectrum sensing method encompasses both downlink and uplink transmissions. However, for the purposes of evaluating the proposed method in this study, we focus solely on uplink transmission. Consequently, a dataset was generated specifically for our experimental analysis. MATLAB [11] is utilized to simulate and construct the synthetic NOMA uplink dataset. The detailed procedure for data generation is elucidated as follows.

We consider Q PUs transmitting simultaneously using NOMA and M SUs acting as sensors. During N time samples in each sensing interval, the received signal is collected. The dataset contains K such intervals.

The activity state of PUs at time k is represented as a binary vector:

$$\boldsymbol{\theta}^{(k)} = [\theta_1^{(k)}, \ldots, \theta_Q^{(k)}]^\top, \quad \theta_q^{(k)} \in \{0, 1\}. \tag{7}$$

A. Transmitted Signals

Each PU q transmits symbols with power allocation Ω_q, where $\sum_q \Omega_q = 1$. The baseband signal is modeled as

$$s_q[n] \sim \mathcal{CN}(0, \Omega_q), \quad n = 1, \ldots, N. \tag{8}$$

B. Channel and Noise Model

In the examined uplink NOMA scenario, the communication channel connecting each PU to each SU is presumed to adhere to a flat Rayleigh fading model. The specific flat Rayleigh fading channel bridging PU q and SU m is represented by

$$H_{q,m} \sim \mathcal{CN}(0, 1) \tag{9}$$

Collecting all links, the channel matrix can be expressed as:

$$\mathbf{H} \in \mathbb{C}^{Q \times M} \tag{10}$$

At each SU, the received signal is affected by additive white Gaussian noise (AWGN) [12], which serves as a model for thermal noise as well as other independent background interference sources. The noise sample at the m-th SU and time instance n is represented as:

$$w_m[n] \sim \mathcal{CN}(0, \sigma_m^2) \tag{11}$$

where σ_m^2 is the variance of the noise. In the simulation presented, it is assumed that all SUs experience unit variance noise (σ_m^2 = 1) for simplicity and normalization.

C. Received Signal

Stacking N samples, the signal matrix received for the k-th snapshot is

$$\mathbf{Y}^{(k)} = \sqrt{\alpha}\, \mathbf{S}\, \mathrm{diag}(\boldsymbol{\theta}^{(k)})\, \mathbf{H} + \mathbf{W}, \tag{12}$$

here $\mathbf{S} \in \mathbb{C}^{N \times Q}$ represents the PU symbol matrix, $\mathrm{diag}(\boldsymbol{\theta}^{(k)})$ encodes PU activity pattern, $\mathbf{H}$ denotes the channel gain, and $\mathbf{W} \in \mathbb{C}^{N \times M}$ corresponds to additive noise.

D. Signal-to-Noise Ratio (SNR)

The SNR is defined as the ratio of average received signal power, P_s to average noise power, P_n:

$$SNR = \frac{\mathbb{E}[P_s]}{\mathbb{E}[P_n]} \tag{13}$$

Since P_s and P_n vary randomly, a scaling factor α is applied to normalize the received signal to the desired target $SNR = 10^{\mathrm{SNR}_{dB}/10}$, which is

$$\alpha = \frac{\mathrm{SNR}}{P_s/P_n}, \quad SNR = \frac{\alpha P_s}{P_n} \tag{14}$$

This guarantees that the effective SNR, after the scaling process, aligns precisely with the predetermined value.

E. Labels

Every predictive unit activity vector, as referenced in $\boldsymbol{\theta}^{(k)}$, is correspondingly assigned an integer label:

$$\theta_{\text{label}}^{(k)} = \sum_{q=1}^{Q} \theta_q^{(k)} 2^{q-1}. \tag{15}$$

For $Q = 2$, the classes are $\{00, 01, 10, 11\} \rightarrow \{0, 1, 2, 3\}$.

The ultimate dataset comprises correlation metrics $\mathrm{CC} \in \mathbb{R}^{K \times 2 \times M \times M}$ as features and PU activity states $\theta \in \{0, \ldots, 2^Q - 1\}^K$ as labels. Consequently, the dataset encapsulates the spatio-temporal statistics of received signals amidst fluctuating PU activity patterns, channel realizations, and noise conditions.

IV. Proposed Model

In this study, we used hybrid quantum convolutional neural networks (HQCNN) to identify active users within CRNs. The received signals are transformed into a two-dimensional covariance matrix, which serves as an analogous image input for our HQCNN model to detect spectrum holes in the network. Our model architecture leverages the VQC for training the model as shown in Fig. 2. Our data generated from the simulation as explained in Section III go through CNN backbone layers that extract classical features. Then the classical features are processed for a quantum circuit. After processing, the main quantum training is performed which here in Fig. 2 is mentioned as VQC consisting of multiple variational layers. Each variational layer consists of angle embedding and entanglement with the input data reuploading technique. Finally VQC measurements results in the generation of classical values corresponding to quantum states.

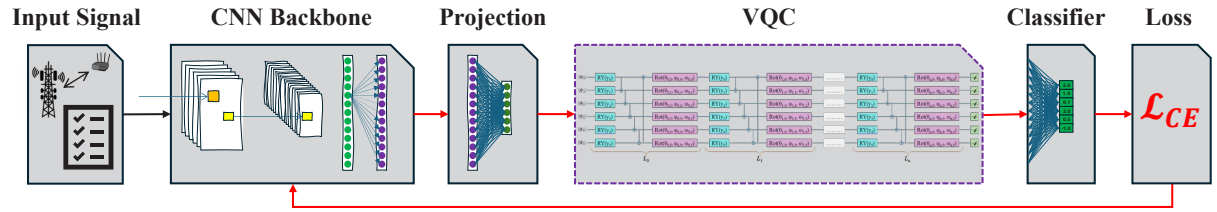

Fig. 2. Model architecture showing classical and quantum processing components.

These classical values are subsequently processed through a classical classifier, after which a loss function is applied to facilitate the training of the parameters. All components of the proposed model will be discussed in the following.

TABLE I
CNN LAYER SHAPES AND PARAMETER COUNTS.

Layer	Output shape	# Params
Conv2d $(2 \to 12, 5\times5)$ + Tanh	$12 \times 28 \times 28$	612
MaxPool2d (2×2)	$12 \times 14 \times 14$	0
Conv2d $(12 \to 32, 5\times5)$ + Tanh	$32 \times 14 \times 14$	9,632
MaxPool2d (2×2)	$32 \times 7 \times 7$	0
Flatten	1,568	0
Linear $(1{,}568 \to 120)$ + Tanh	120	188,280
Linear $(120 \to 84)$ + Tanh	84	10,164
Linear $(84 \to 32)$ + Softmax	32	2,720
Total		**211,408**

A. CNN Backbone

Due to the high dimensionality and inherent noise of the raw input signals, a CNN backbone is employed to extract meaningful and robust representations prior to quantum processing. The architecture of this network is summarized in Table I.

The CNN consists of two convolutional layers with Tanh activations, each followed by max pooling, after which the output is flattened into a 1,568-dimensional vector. This vector is passed through three fully connected layers ($1,568 \to 120 \to 84 \to 32$), where the first two employ Tanh and the final layer applies Softmax. The resulting 32-dimensional vector serves as the final feature embedding, defined

$$z \in \mathbb{R}^d, \quad d = feature\_dim = 32 \tag{16}$$

This embedding is then forwarded into the subsequent quantum stage.

B. Classical-Quantum Projection

In quantum computing, a qubit state lives in Bloch sphere as in Eq. 17

$$|\psi\rangle = cos(\frac{\theta}{2})\,|0\rangle + e^{i\phi} sin(\frac{\theta}{2})\,|1\rangle \tag{17}$$

In our proposed model we used VQC, that employ rotations around the axes of the Bloch sphere on each qubit. RY angle embedding is used in our proposal, which is single-qubit rotation gate around y-axes:

$$R(\tfrac{\theta}{2}) = \begin{bmatrix} \cos\frac{\theta}{2} & \sin\frac{\theta}{2} \\ -\sin\frac{\theta}{2} & \cos\frac{\theta}{2} \end{bmatrix} \tag{18}$$

In Eq. 18, the input θ to the quantum circuit must be a real parameter. Thus, we present this projection layer delineated in Eq. 19, which is designed to be learnable. It optimally compresses the feature space $\mathbb{R}^d$ to the quantum encoding space $\mathbb{R}^n$.

$$s = Wz + b \tag{19}$$

Where CNN produces input $z \in \mathbb{R}^d$, $W \in \mathbb{R}^{n\times d}$ is the weight matrix, $b \in \mathbb{R}^n$ is the bias, and $n =$ the number of qubits. Thus far, the progression can be delineated as follows:

$$input \xrightarrow{CNN} z \in \mathbb{R}^d \tag{20}$$

$$\xrightarrow{Projection} s \in \mathbb{R}^n \tag{21}$$

$$\xrightarrow{angle=s_i} |0\rangle^{\otimes n} \xrightarrow{RY(s_i)} |\psi\rangle \tag{22}$$

C. VQC with data re-uploading model

The core of the proposed quantum neural network (QNN) is the VQC. Additionally, the data re-uploading technique is employed to improve accuracy, enabling single-qubit models to achieve neural-network-level expressiveness despite the no-cloning limitation [13]. In our proposed VQC model as depicted in Fig. 3, we used 6-qubit VQC with data reupload. While conventional VQCs rely solely on fixed parameterized gates, our model incorporates the input data at each variational layer. Detailed VQC architecture will be discussed next.

The variational layer L_i within our proposed VQC is composed of three distinct components, as delineated below.

a) Input encoding: Classical data are encoded into quantum states using rotation about y axes in the Bloch sphere following Eq. 18. In Fig. 3, aqua colored quantum gates shown for this angle encoding where $y_i = y_1, y_2, ..., y_n$ are the angle of RY gates. Each qubit face with angle encoding y_i that was generated from the projection layer using Eq. 19.

b) Subsequent to angle encoding, CNOT gates are applied to each qubit to ensure entanglement. Here, the target qubit is iteratively designated as the qubit following the control qubit in a circular manner.

$$CNOT(|\psi_0\rangle \to |\psi_1\rangle), CNOT(|\psi_1\rangle \to |\psi_2\rangle), \ldots,$$
$$CNOT(|\psi_{n-1}\rangle \to |\psi_n\rangle), CNOT(|\psi_n\rangle \to |\psi_0\rangle) \tag{23}$$

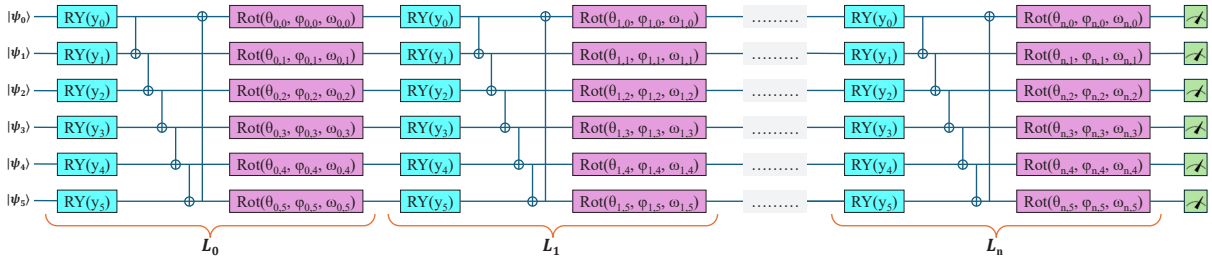

Fig. 3. Variational quantum circuit (VQC) with data re-uploading.

c) Finally the variational part of the VQC layers shown in purple in Fig. 3. Where $Rot()$ is expressed as follows:

$$Rot(\theta, \phi, \omega) = R_z(\omega)R_y(\theta)R_z(\phi) \tag{24}$$

Each qubit $|\psi_i\rangle$ at layer l has its own trainable parameters $(\theta_{l,i}, \phi_{l,i}, \omega_{l,i})$.

After applying n variational layers, a quantum measurement is performed, yielding a probabilistic outcome over the possible eigenstates and converting the quantum state into its classical representation.

D. Classifier

Upon completion of the quantum measurement process, it yields 2^{n_qubits} distinct eigenstates. The probability distribution of these eigenstates may not correspond directly to the established classification categories. To match the dimensionality of the classification labels, the measured outputs are passed through a fully connected layer, followed by a Softmax function (Eq. 25) to select the most probable class.

$$p_{i,c} = \frac{e^{z_{i,c}}}{\sum_{j=1}^{C} e^{z_{i,j}}}, \quad c = 1, ..., C = classes \tag{25}$$

E. Loss Function

In the training loop, cross entropy loss function was utilized. Eq. 26 applied for our model cross entropy loss for sample (x_i, y_i) and batch size B.

$$\mathcal{L}_{CE} = -\frac{1}{B}\sum_{i=1}^{B} log(p_{i,y_i}) \tag{26}$$

To optimize the parameters, an Adam optimizer with a learning rate of $\eta = 1 \times e^{-3}$ was used.

V. Experimental Results and Discussion

To evaluate the performance of our proposed model, we compared it with some of the cutting edge models. The baselines are: DS2MA: a Deep Spectrum Sensing with Multi-Antenna [5], and CNN-NOMA: CNN-based Spectrum Sensing for NOMA) [4], CNN-SαS: CNN-based Spectrum Sensing under Symmetric α-Stable noise) [6]. These methods serve as robust benchmarks in the domains of spatial diversity, noise robustness, and enhanced detection for NOMA, respectively. To ensure fair comparison, all baseline models architecture were kept as it is just input and classification classes are adjusted with our simulation.

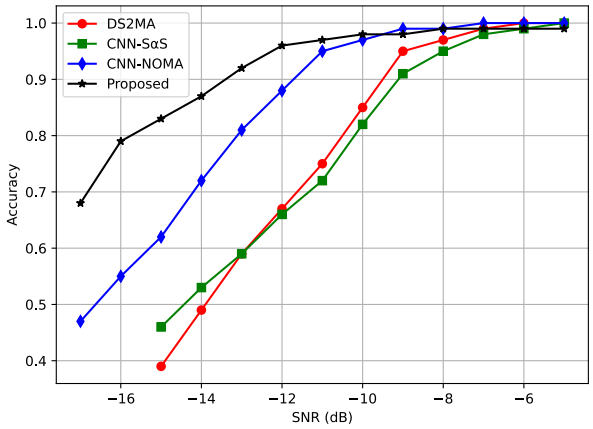

Fig. 4. Accuracy comparison of proposed model with baseline methods across different SNR levels.

Fig. 4 shows the proposed model's sensing accuracy compared to the baseline. The accuracy of different models are present on SNR levels ranging from -18 dB to -4 dB. The proposed model demonstrates an accuracy of 90% or greater at an SNR level of -13 dB, whereas the nearest competitor, CNN-NOMA, achieves the same level of accuracy at -12 dB. The remaining methodologies exhibit comparable accuracy levels once the SNR exceeds -9 dB. CNN-NOMA exhibits substantially improved performance within low to mid-SNR ranges compared to DS2MA and CNN-SαS. However, it remains inferior to the proposed model at very low SNR levels. The black line plot in Fig. 4 shows clear understanding that the proposed model outperforms all baselines in the low SNR regime (-17 to -12 dB), where spectrum detection is the most challenging. At high SNRs of -8 dB and above, the performance of the proposed model converges with that of CNN-NOMA, attaining nearly perfect accuracy.

In this study, our second experiment was a comparison of the detection probability for PUs as a function of SNR shown in Fig. 5. The results show that the proposed model consistently outperforms the baselines, particularly in the low SNR regime. CNN-NOMA performs well at mid-to-high SNR, while DS2MA and CNN-SαS improve with higher SNR. The

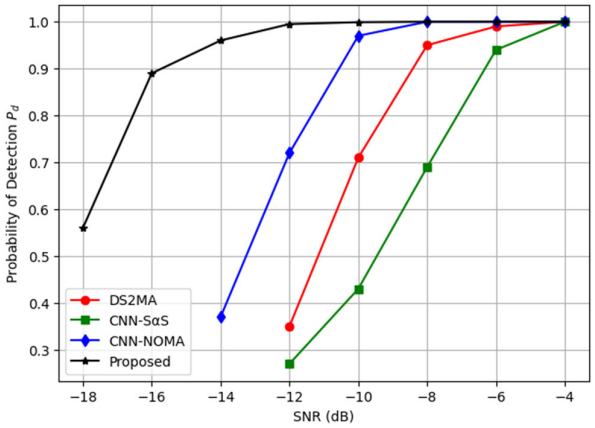

Fig. 5. Detection performance comparison across SNR levels for PU_1.

proposed approach excels with near-optimal detection at very low SNR, showcasing robustness in noisy environments.

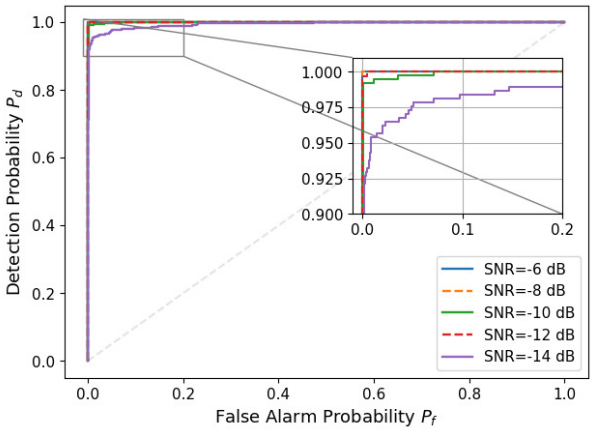

Fig. 6. ROC curves of detection probability versus false alarm probability at different SNR levels.

The ROC provide a comprehensive evaluation of the detection performance under varying decision thresholds. Fig. 6 shows the ROC curves for six SNR levels of our model as used in PU_1, illustrating the relationship between detection probability and false alarm probability. The proposed model consistently demonstrates improved detection probabilities across all levels of SNR. The curves yield a substantial area under the curve (AUC), even at low SNR, corroborating the model's superior detection capabilities and robustness.

Another comparison metric could be the complexity of the models. While maintaining an identical simulation setup, the models implemented in DS2MA and CNN-SαS demand a considerable number of trainable parameters, specifically 93.57 million and 37.92 million, respectively. In contrast, the CNN-NOMA model requires 243,648 parameters, whereas the proposed model demonstrates enhanced efficiency by requiring only 211,634 trainable parameters.

VI. Conclusion

We have introduced a quantum sensing mechanism tailored for wideband spectrum sensing. The core component of this mechanism is a VQC that leverages data reuploading within its variational layer. Additionally, it employs CNN head to extract classical features. Simulations were performed to generate uplink data using the CRN-NOMA architecture, which was subsequently used for both training and validation of the model. Ultimately, our approach was compared to the state-of-the-art baselines. In terms of sensing accuracy, detection probability, false alarm probability, and parameters relevant to model training, the proposed model demonstrated superiority in the general sense. Furthermore, our experiment demonstrates that the proposed model is more effective in challenging noise-dominated environments at low SNR, offering significant accuracy gains over baselines.

References

[1] D. Yadav, S. Majumder, and A. Raghuvanshi, "Fcm based spectrum sensing for noma cognitive radio networks," in *2024 2nd World Conference on Communication & Computing (WCONF)*, pp. 1–6, 07 2024.

[2] A. Kumar, A. Nanthaamornphong, and M. Masud, "Rnn-bi-lstm spectrum sensing algorithm for noma waveform with diverse channel conditions," *Scientific Reports*, vol. 15, p. 31022, Aug 2025.

[3] J. Wu, T. Xu, T. Zhou, X. Chen, H. Hu, and C. Wu, "Adaptive NOMA-based spectrum sensing for uplink IoT networks," *IEEE Transactions on Cognitive Communications and Networking*, vol. 10, no. 1, pp. 138–149, 2024.

[4] S. Majumder, "Convolutional neural network-based spectrum sensing for NOMA cognitive radio networks," *Digital Signal Processing*, vol. 163, p. 105243, 2025.

[5] K. Chae and Y. Kim, "Ds2ma: A deep learning-based spectrum sensing scheme for a multi-antenna receiver," *IEEE Wireless Communications Letters*, vol. 12, no. 6, pp. 952–956, 2023.

[6] A. Mehrabian, M. Sabbaghian, and H. Yanikomeroglu, "Spectrum sensing for symmetric α-stable noise model with convolutional neural networks," *IEEE Transactions on Communications*, vol. 69, no. 8, pp. 5121–5135, 2021.

[7] L. X. Nguyen, A. D. Raha, P. S. Aung, D. Niyato, Z. Han, and C. S. Hong, "A contemporary survey on semantic communications: Theory of mind, generative ai, and deep joint source-channel coding," *IEEE Communications Surveys & Tutorials*, pp. 1–1, 2025.

[8] S. E. Abdelbaset, A. A. El-Shafie, M. A. Tawfik, and H. M. A. Fahmy, "Deep learning-based spectrum sensing for cognitive radio applications," *Sensors*, vol. 24, no. 24, p. 7907, 2024.

[9] R. Piron and C. Goursaud, "Quantum annealing for active user detection in NOMA systems," in *Proc. 58th Asilomar Conf. Signals, Systems, and Computers*, (Pacific Grove, CA, USA), pp. 1448–1452, 2024. Also available as arXiv:2411.05411.

[10] B. Narottama, D. K. Hendraningrat, and S. Y. Shin, "Quantum-inspired evolutionary algorithms for noma user pairing," *ICT Express*, vol. 8, no. 1, pp. 11–17, 2022.

[11] The MathWorks, Inc., "Matlab version r2025a." The MathWorks, Inc., 2025. URL: https://www.mathworks.com.

[12] A. b. Idris, R. F. b. Rahim, and D. b. M. Ali, "The effect of additive white gaussian noise and multipath rayleigh fading on ber statistic in digital cellular network," in *2006 International RF and Microwave Conference*, pp. 97–100, 2006.

[13] A. Pérez-Salinas, A. Cervera-Lierta, E. Gil-Fuster, and J. I. Latorre, "Data re-uploading for a universal quantum classifier," *Quantum*, vol. 4, p. 226, Feb. 2020.